In-situ tension investigation of additively manufactured silver lines on flexible substrates

Seungjong Lee^{1,2}, Zabihollah Ahmadi³, Mikyle Paul^{1,2}, Masoud Mahjouri-Samani^{2,3}, Shuai Shao^{1,2}, Nima Shamsaei^{1,2*}

¹ Department of Mechanical Engineering, Auburn University, Auburn, AL 36849, USA

² National Center for Additive Manufacturing Excellence (NCAME), Auburn University,

Auburn, AL 36849, USA

³ Electrical and Computer Engineering Department, Auburn University, Auburn, AL, 36849, USA

*Corresponding Author:

Email: shamsaei@auburn.edu

Tel: 334.844.4839

Submitted to:

Additive Manufacturing Letters

June 2023

Abstract

The reliability of additively manufactured flexible electronics or so-called printed electronics is defined as mean time to failure under service conditions, which often involve mechanical loads. It is thus important to understand the mechanical behavior of the printed materials under such conditions to ensure their applicational reliability in, for example, sensors, biomedical devices, battery and storage, and flexible hybrid electronics. In this article, a testing protocol to examine the print quality of additively nanomanufactured electronics is presented. The print quality is assessed by both tensile and electrical resistivity responses during in-situ tension tests. A laser based additive nanomanufacturing method is used to print conductive silver lines on polyimide substrates, which is then tested in-situ under tension inside a scanning electron microscope (SEM). The surface morphology of the printed lines is continuously monitored via the SEM until failure. In addition, the real-time electrical resistance variations of the printed silver lines are measured insitu with a multimeter during tensile tests conducted outside of the SEM. The protocol is shown to be effective in assessing print quality and aiding process tuning. Finally, it is revealed that samples appearing identical under the SEM can have significant different tendencies to delaminate.

Keywords: Additive nanomanufacturing; Dry printing; Flexible hybrid electronics; In-situ mechanical testing; Testing protocol; Qualification

Nomenclature & Abbreviations

AJP	Aerosol-jet printing	
AM	Additive manufacturing	
ANM	Additive nanomanufacturing/Additively nanomanufactured	
EDS	Energy dispersive spectroscopy	
IJP	Ink-jet printing	
SEM	Scanning electron microscope/microscopy	

1. Introduction

Additive manufacturing (AM), a layer-by-layer fabrication process, is already utilized in biomedical and aerospace applications with various benefits, such as rapid prototyping, the ability to fabricate complex structures, and near-net-shape production [1], [2]. To harness the aforementioned advantages for electronics and sensors, some AM techniques, such as ink-jet printing (IJP) and aerosol-jet printing (AJP), have been developed [3], [4], [5]. These direct-writing techniques are not only able to overcome the limitations of conventional device manufacturing processes, such as excessive wastage and infeasibility of fabrication on flexible and stretchable substrates, but also to fabricate embedded, 3D structural and conformal electronics [6], [7], [8], [9], [10], [11]. IJP and AJP are ink-based processes [12], [13], [14], [15], [16], [17]. Limitations in the material selection due to the complexity of ink formulation, non-purity of ink due to the existence of polymers/additives [18], and post-processing needed for removing the polymers/additives from the ink are among the disadvantages of these printing technologies. Recently, a new additive nanomanufacturing (ANM) and dry printing technique has emerged [19], [20], [21], [22] as a promising method for printing various electronics and sensors.

The ANM technique has been successfully demonstrated to print various patterns, electronic circuits, and sensors. In this printing technique, nanoparticles of different materials are generated on demand using a pulsed laser ablation technique, followed by a real-time laser sintering process. The ANM technique is capable of generating dry and contamination-free (solvent-free) nanoparticles as well as printing multimaterial and hybrid structures at room temperature and atmospheric pressure on various substrates, including flexible polyimide. The surface morphologies of ANM-printed materials are similar to those fabricated by IJP and AJP, although ANM is a dry printing process unlike IJP and AJP [23], [24], [25]. An investigation on

the mechanical reliability of the additively nanomanufactured (ANM) samples by measuring the electrical resistance of printed lines before and after cyclic bending and stretching tests confirmed that the samples were still conductive similar to the results from IJP [23]; the resistivity only increased by less than double, provided the ANM materials were still attached well after testing [19].

Like any AM processes, the ANM process parameters require extensive tuning to reach the optimum processing condition—one of many indicators for which is the adhesion integrity between the substrate and the printed material. Indeed, the primary application of the ANM technique, i.e., flexible electronics, is susceptible to delamination due to the mismatch in elastic modulus between the substrate and printed materials which can result in circuit failure [26]. Therefore, the adhesion stability, often measured as the substrate's tensile strain at which delamination occurs (i.e., delamination strain) is of special interest. This property is perhaps as important as the integrity under cyclic load since it indicates the printed electronics' resistance to failure when an unexpectedly high deformation (i.e., overload) is experienced [27]. Although static tension test is the most intuitive for measuring the delamination strain, quantifying this property is still challenging since the initial onset of such damage is often invisible to the naked eye or even to optical microscopy. This is not only because of the microscopic nature of the damage, but also the printed materials, such as Ag and Cu, being opaque to visible light and often highly reflective.

This study put forth an in-situ testing protocol for evaluating the print quality of ANM flexible electronics, which measures both delamination tensile strain and the evolution of resistivity during tensile loading. Using an in-situ loading module, quasi-static tension was applied inside a scanning electron microscope (SEM) to capture any physical changes such as crack initiations/propagations, and material delamination during the tests. Using live image capture, the

instantaneous delamination strains were measured. In addition, electrical resistivity measurements were performed in-situ during tensile tests conducted outside of the SEM, to evaluate the sensitivity of resistivity to tensile deformation and/or delamination.

2. Methodology

The proposed protocol to examine the print quality of ANM flexible electronics comprises steps of (1) surface examination of printed lines within the SEM; (2) in-situ tensile test within the SEM; and (3) in-situ tensile test with electrical resistivity monitoring outside of the SEM. Well-fused metallic print lines typically possess evenly distributed particles that sufficiently cover the entire printing area which are consolidated via solid state fusion. Insufficient materials or over/under heating from the laser can all lead to print anomalies and compromised structural integrity. Thus, Step (1) serves as to prescreen the samples for such obvious print anomalies. Samples that pass Step (1) proceed to Steps (2) and (3). The prime indicator of print quality is the delamination strain – ideally, the delamination strain should be greater than the fracture strain of the substrate. These steps of the protocol involve scanning electron microscopy, in-situ tensile testing within the SEM, and tensile testing with in-situ electrical resistivity monitoring. These components, together with the fabrication procedure of the ANM samples, are outlined in the sections below.

2.1. Fabrication

The schematic illustration of the ANM printer is presented in **Figure 1**(a). It consists of a microchamber, a rotating target, a nozzle, and a gas flow feeder system. A pulsed laser (Coherent COMPex excimer laser) was divided into two paths for ablation and sintering by a beam splitter. The silver target was ablated by the laser; and nanoparticles were generated in-situ under the Ar environment. The nanoparticles were then directed toward the substrate through a 400 µm nozzle

using an Ar carrier gas, where they were sintered using a 5 W continuous wave laser in real-time. By moving the XY positioning stage according to the preprogrammed path, the material was deposited on the substrate and sintered by the laser. More details regarding the ANM fabrication process can be found in the previous works by the authors [19], [20]. Polyimide sheets with a thickness of ~175 μm were used as the substrates; and were laser cut into dog bone shapes with 2 mm by 2 mm square gage sections so that the entire gage was observable within the SEM's field of view. Laser cutting was used to prepare the polyimide substrates to prevent the formation of cracks or notches on the edges. Polyimide is a commonly used material for flexible electronics substrate due to its excellent heat and chemical resistance.

A shoulder with a large radius of 30 mm was used to minimize stress concentration. The grip width, length, and total sample length of 8 mm, 7 mm, and 42 mm, respectively, were selected to be compatible with the in-situ tensile module configuration. The geometry of the dog bone shaped substrates is presented in **Figure 1**(b). Ag nanoparticles were deposited and sintered within a 6 mm by 2 mm rectangle on the gage section of each sample, as shown in **Figure 1**(c). Two different sets of process parameters were selected by varying the sintering power. Both sets of process parameters resulted in similar surface morphologies without debonding and substrate damage. The details of process parameters are listed in **Table 1**.

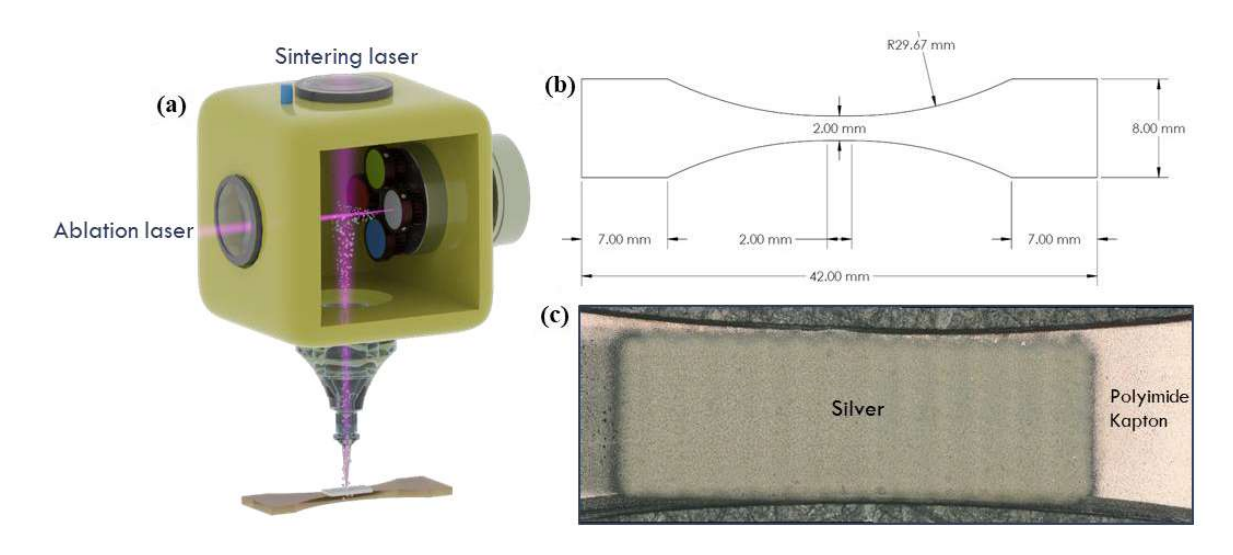


Figure 1 (a) The schematic illustration of the ANM printer. (b) The geometry of dog bone polyimide substrate. (c) Printed Ag rectangle on the middle section of the dog bone polyimide substrate.

Table 1 Details of selected process parameters.

Set	Scanning Speed (mm/s)	Pass Count (#)	Hatching Distance (µm)	Sintering Power (W)
#1	10	10	100	2
#2	10	10	100	1

2.2. Mechanical testing

The tension-compression module provided by Kammrath & Weiss with a 2 kN load cell and Zeiss Crossbeam 550 SEM were utilized for in-situ tensile tests. The testing system configurations before and after mounting the module within the SEM stage are presented in **Figure 2**. The printed samples were placed on the grips before installing the in-situ module inside the SEM (shown in **Figure 2**(a)). The distance between the upper and lower grips was adjusted, and the sample was gripped (shown in **Figure 2**(b)). After the sample was secured within the grips, the module was placed on the SEM stage (shown in **Figure 2**(c)). Any compressive or tensile loads induced during the gripping process were relieved by setting the applied load to 0 N. SEM images

were captured using a voltage of 5 kV and a current of 100 pA. In addition, the elemental analysis of deposited material on the gage section was performed using energy dispersive spectroscopy (EDS) in the SEM with a working distance of 5 mm, a voltage of 5 kV, and a current of 100 pA.

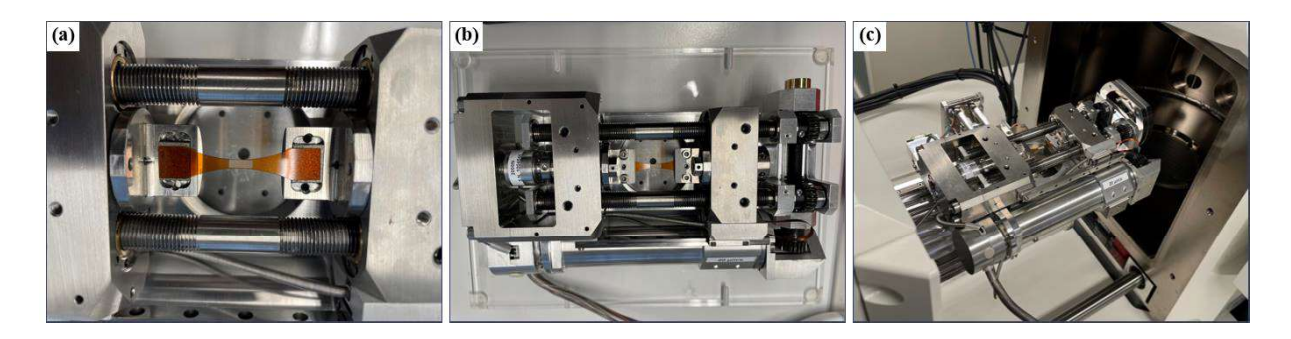


Figure 2 The test system configurations before and after mounting the tension-compression module on the SEM stage: (a) placing the sample on the grips, (b) gripping the sample, and (c) placing the module on the SEM stage.

Quasi-static tensile tests were conducted under displacement-control in both intermittent and continuous modes. The intermittent mode proceeded with both 250 µm and 500 µm displacement intervals and the image of the sample surface was captured by SEM at each interval. Therefore, a total of three in-situ tensile tests (i.e., 250 µm intervals, 500 µm intervals, and continuous) were conducted. Different displacement intervals were investigated due to the force relaxation observed during pausing for image capture to confirm whether the observed relaxation had any effect on the electrical resistivity and the printed line integrity. While the surface of the printed material was examined at various magnifications (15-1000X) before tensile tests, only a fixed magnification of 40X was used during the tests. The tension-compression module was controlled using the software provided by Kammrath & Weiss. This software also recorded displacement and force readings for each test.

2.3. Electrical resistance measurements

Additional tensile tests were conducted outside of the SEM using the same tension-compression module to measure electrical resistance during tensile loading. For intermittent tests with 250 µm and 500 µm displacement intervals, the electrical resistance was measured by a multimeter at each interval. **Figure 3** illustrates the technique employed for measuring the electrical resistance of the printed Ag lines during mechanical testing. Three additional tensile tests were conducted using different intervals (i.e., 250 µm intervals, 500 µm intervals, and continuous), which reflected the same testing schedules used for tensile tests within the SEM. The change in the electrical resistance during continuous tests was also measured by continuously capturing and logging the multimeter data. Both tensile tests conducted inside and outside of the SEM at the same loading intervals were considered equivalent tests as the loads were identical, although the environment was different; i.e., in vacuum within the SEM, and at atmospheric conditions outside the SEM.

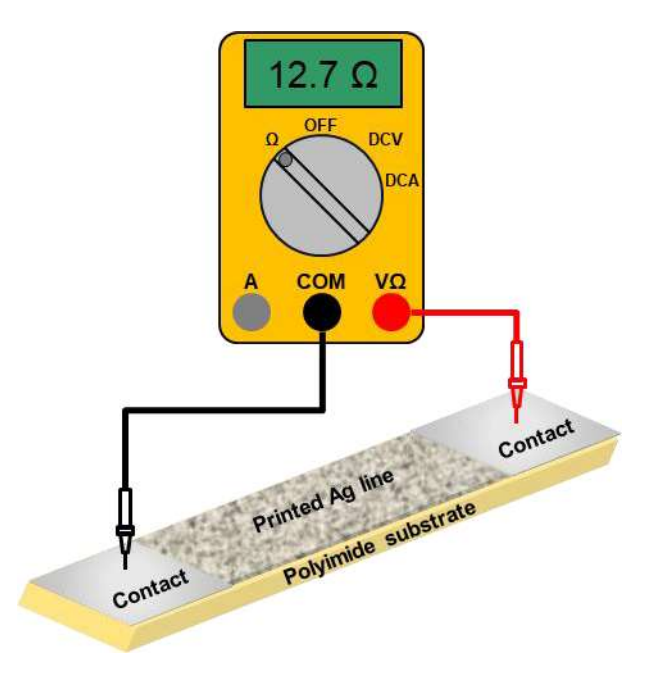


Figure 3 A schematic illustrating the measurement of electrical resistance of printed Ag lines during tests.

3. Results and discussions

3.1. Surface morphology and microstructures of the printed materials

The gage section surface of a sample fabricated with process parameters Set #1 captured by SEM at different magnifications is presented in **Figure 4**. The surface morphology of the sample fabricated with Set #2 was nearly identical, as presented in **Figure S1** in the supplementary material. The sintered Ag rectangle covered the entire gage section, as shown in **Figure 4**(a). A previous study from the authors' group showed that the printed lines can have higher porosity if the laser sintering energy is insufficient to fuse nanoparticles [19]. **Figure 4**(b) confirmed that the laser sintering energy used in this study was appropriate to fuse Ag nanoparticles together without apparent porosity. In addition, when the laser sintering energy is excessive, the surface melts and tends to develop cracks due to tensile residual stresses formed during re-solidification [19]. **Figures 4**(c) and (d) shows that the printed Ag line contained evenly distributed nanoparticles, was not molten in appearance, and did not develop solidification-induced cracks. The elemental analysis results from EDS are presented in **Figure 5**. According to **Figures 5**(b) and (e), ~98.4% of the elements on the scanned surface was silver.

Surface morphology and EDS results can provide a visual clue as to what constitutes a good quality of deposition. However, without the application of a load, it is not possible to validate which of these process parameters are optimized for realistic applications based on adhesion stability. In order to assess the print quality in terms of adhesion stability, the proposed in-situ inspections under tensile loading are therefore suggested.

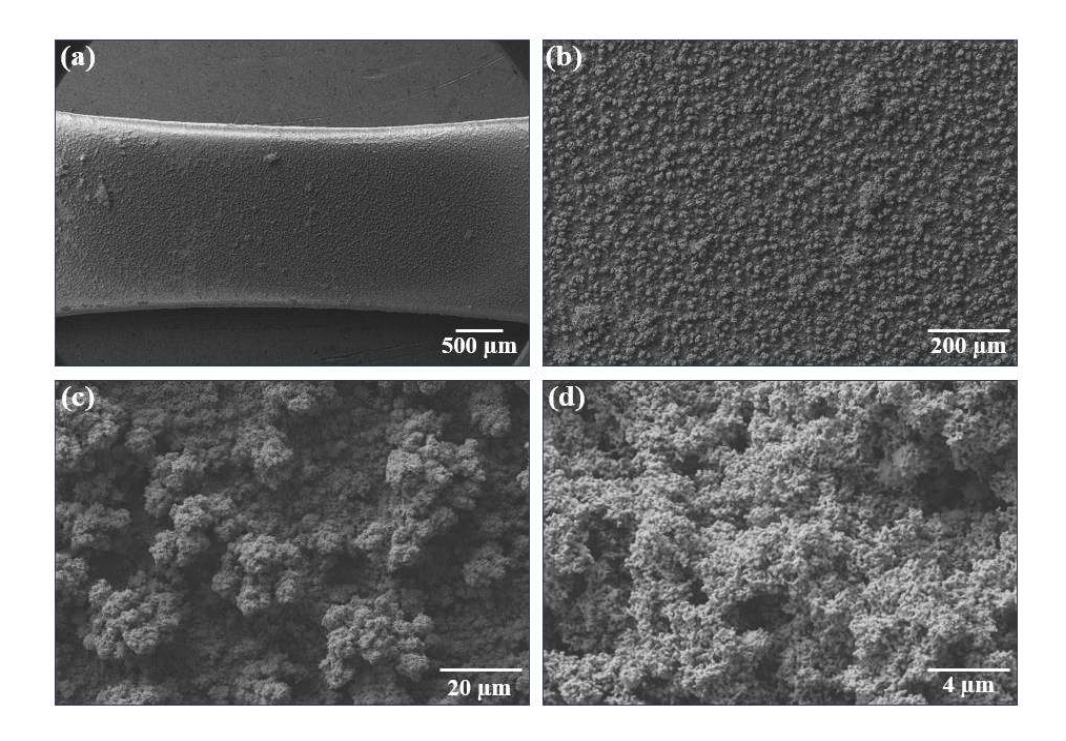


Figure 4 The gage section surface of a sample fabricated with process parameters Set #1 captured by SEM using (a) 23X, (b) 100X, (c) 1000X, and (d) 5000X magnifications.

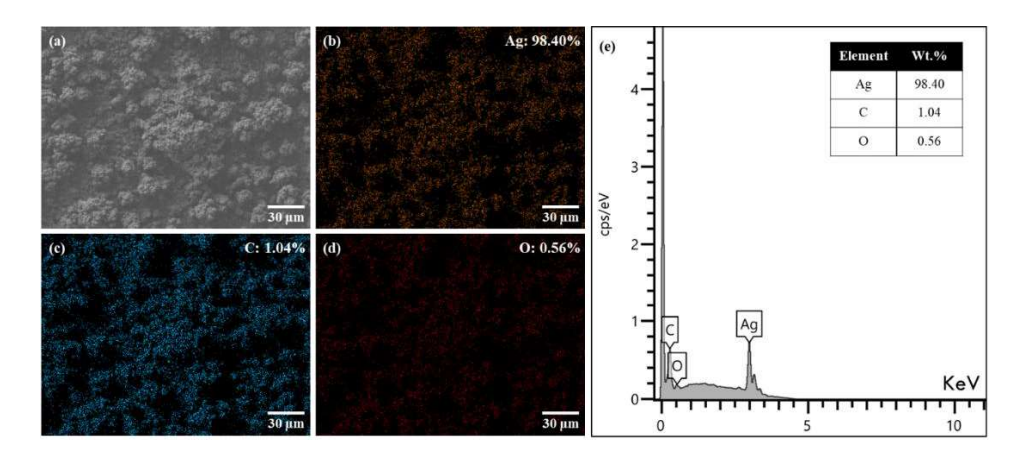


Figure 5 Elemental analysis results obtained from EDS: (a) electron microscopy image of the surface with elemental maps of (b) Ag, (c) C, (d) O, and (e) X-ray photon energy spectrum showing the distribution of elements.

3.2. Tensile response during in-situ tension tests

The SEM images of a sample fabricated using process parameters Set #1, and the force-displacement plot for the intermittent tensile test at 250 µm displacement intervals are presented in **Figures 6**(a)-(i) and (j), respectively. In addition, the SEM images and force-displacement plot during the test at 500 µm displacement intervals are presented in **Figures 7**(a)-(f) and (g), respectively. Furthermore, the SEM video recorded during a continuous tensile test without intervals is presented in the supplementary material (i.e., **Video S1**). The SEM images (i.e., **Figures 6**(a)-(i) and **Figures 7**(a)-(f)) indicate that the adhesion of the sintered Ag line was sufficient and did not delaminate up to substrate fracture, although multiple localized cracks initiated at the edges of the printed material. These observations confirm that the printed Ag lines on the substrate are stable for significant elongation until the substrate fractures.

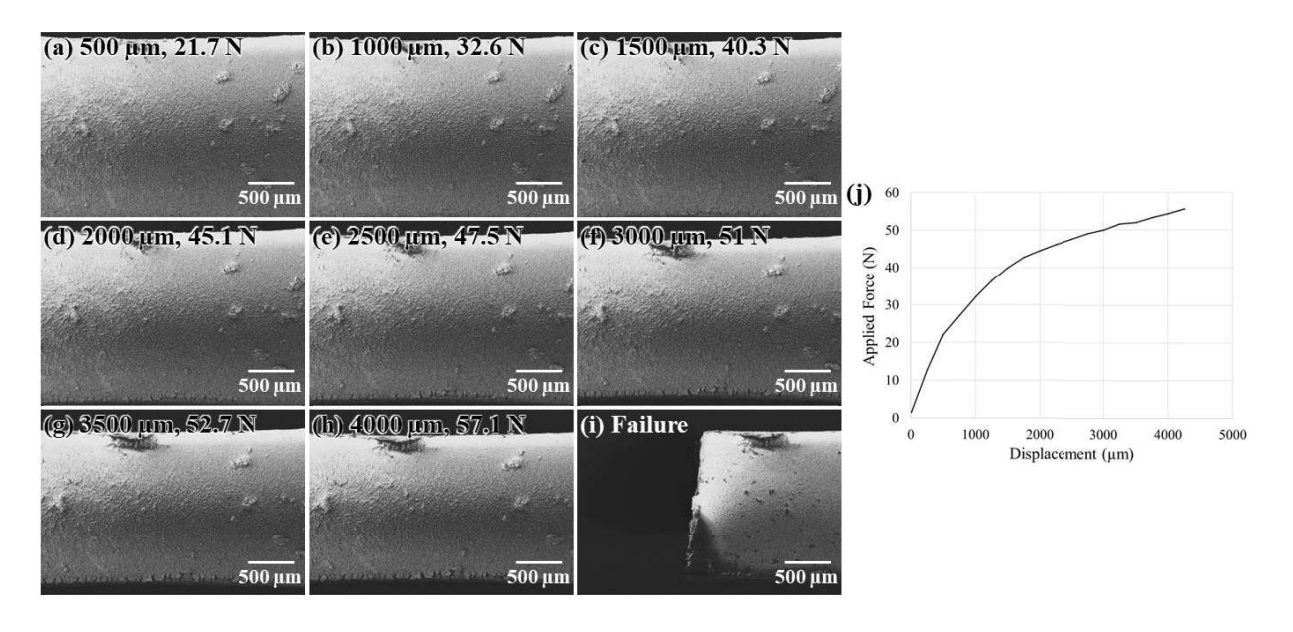


Figure 6 SEM images of samples fabricated using process parameters Set #1 at the displacements of (a) 500 μ m, (b) 1000 μ m, (c) 1500 μ m, (d) 2000 μ m, (e) 2500 μ m, (f) 3000 μ m, (g) 3500 μ m, (h) 4000 μ m, and (i) failure; and (j) the force-displacement plot during tensile test with a 250 μ m displacement interval.

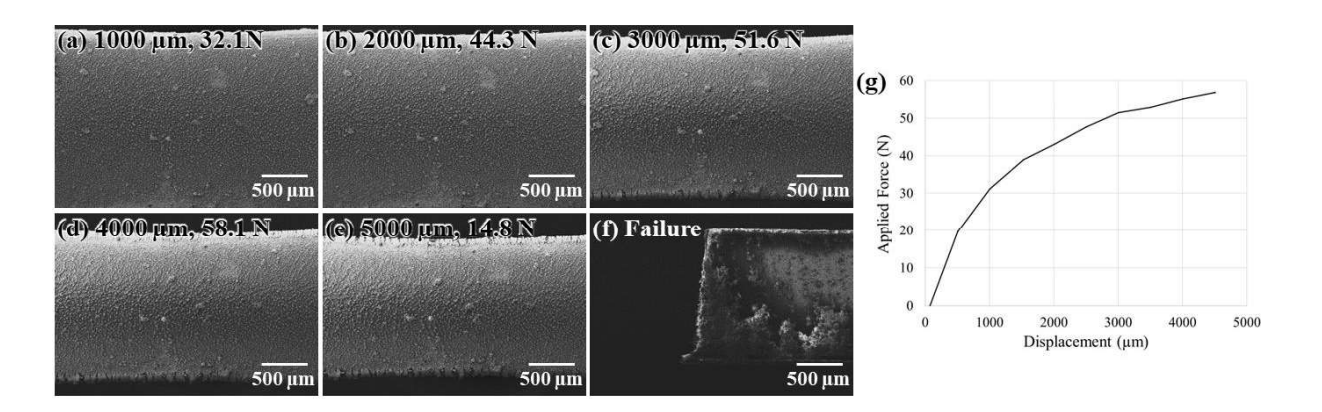


Figure 7 SEM images of samples fabricated using process parameters Set #1 at the displacements of (a) 1000 μ m, (b) 2000 μ m, (c) 3000 μ m, (d) 4000 μ m, (e) 5000 μ m, and (f) failure; and (g) the force-displacement plot during tensile test with a 500 μ m displacement interval.

Force-displacement and force-strain curves of in-situ tensile tests were generated as shown in Figures 8(a) and (b), respectively. The true strain was estimated by considering the relative axial displacement of the features near both ends of the gage section (i.e., larger particles). Only the forces at the beginning of the pause for each interval were shown in Figure 8(b). There are slight differences in estimated fracture force and strains between 250 µm and 500 µm intervals. It may be due to the different number of intermittent pauses during testing that can cause material relaxation. In addition, a tensile test of bare polyimide sample was conducted to investigate the mechanical properties of samples with or without printed materials. The true strain was not calculated for the bare polyimide sample, as the measurement of relative displacement was challenging. Within the SEM, micrographs of the bare polyimide sample could not be obtained due to significant charging issue. Outside of the SEM, direct measurement of strain had to proceed with calipers which may incur significant uncertainty. Therefore, force-displacement curves of samples with printed materials and the bare polyimide sample are presented in Figure 8(a) for comparison. The curves confirm that the printed material does not carry much load, and therefore, does not considerably influence the mechanical properties of the part.

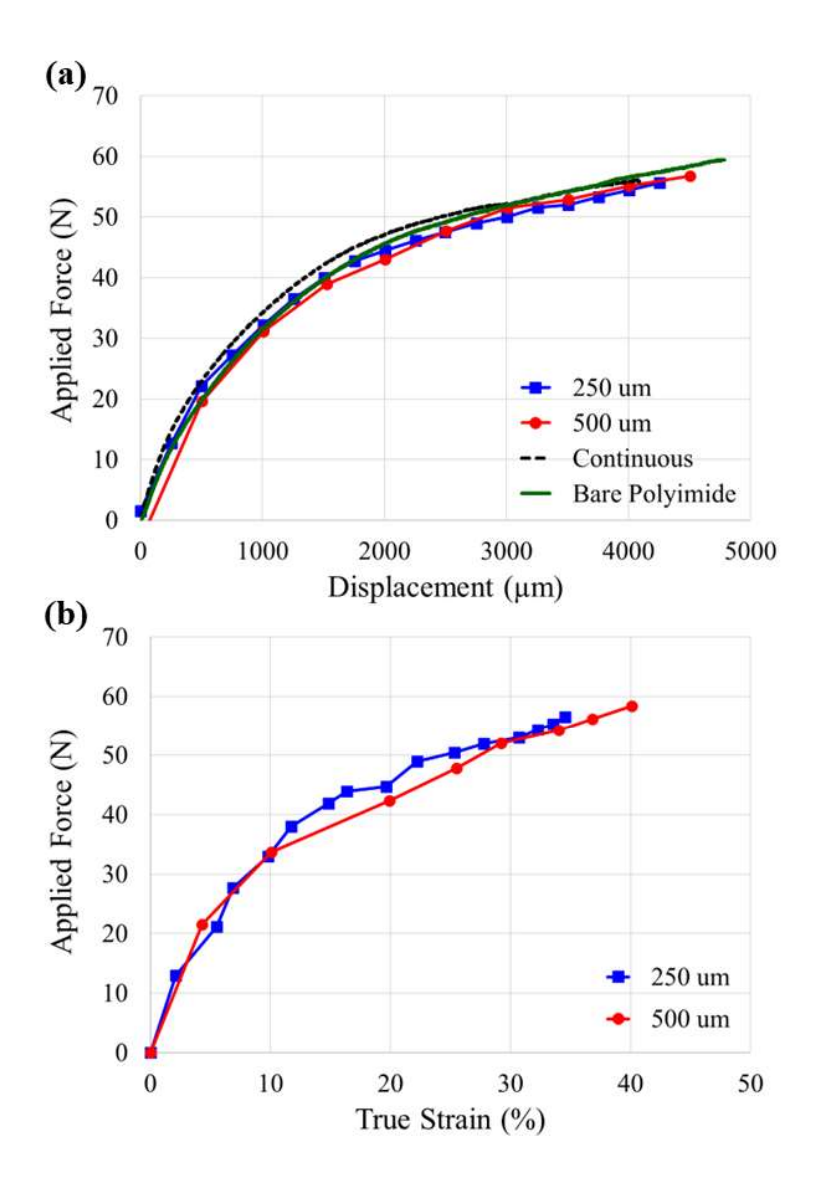


Figure 8 (a) The force-displacement curves of samples with printed materials (i.e., 250 μ m, 500 μ m, and continuous) and continuous tensile test of a bare polyimide sample. (b) The force-strain curves of intermittent tensile tests using two different intervals (i.e., 250 μ m and 500 μ m).

Delamination during tensile tests was observed from the samples fabricated using process parameters Set #2 as presented in **Figure 9**. Apparent delamination ripples appeared when the displacement was over 900 μ m, and the ripple peaks consisted of delaminated material that became larger as displacement increased. As shown in **Figure 9**(a), the precursors of some of these ripples might have appeared as early as 150 μ m. Delamination most likely occurs due to less laser power

resulting in low-quality sintering and also less adhesion to the substrate. To capture more SEM images within the tensile test on the sample fabricated using process parameters Set #2, a smaller displacement interval of $150 \, \mu m$ was used.

Although delamination occurred, the force-displacement response of the sample presented in **Figure 9**(g) did not differ from the samples without delamination shown in **Figure 6**(j) and **Figure 7**(g). The reason is perhaps due to the negligible contribution of the printed Ag lines towards strength. Although surface topographies of both sets before loading were similar, the SEM images during in-situ tensile tests confirmed that the use of process parameters Set #1 did not result in delamination, whereas Set #2 did. It confirmed that the proposed testing protocol, which includes visual inspection under tensile loading, effectively validates the process parameters.

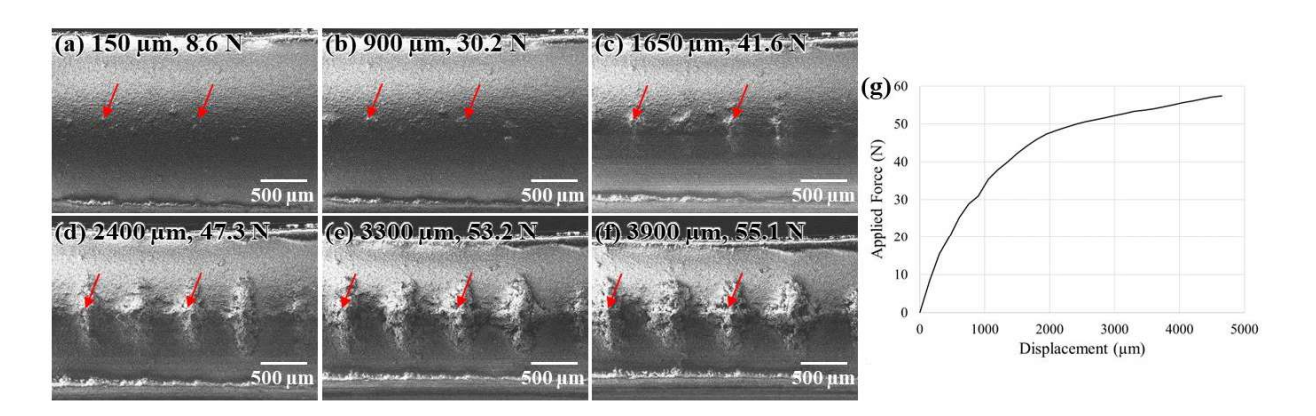


Figure 9 SEM images of a sample fabricated with process parameters Set #1 under tensile test at the displacement of (a) 150 μ m, (b) 900 μ m, (c) 1650 μ m, (d) 2400 μ m, (e) 3300 μ m, and (f) 3900 μ m; and (g) the force-displacement plot during tensile tests with a 150 μ m displacement interval.

3.3. In-situ electrical resistivity response during tension tests

The electrical resistivity-displacement plot of tensile tests conducted on the sample fabricated using process parameters Set #1 (i.e., found to be optimal in Section 3.2) is presented in **Figure 10**. These tests were performed outside of the SEM since electrical resistance could not

be measured within it. For intermittent tensile tests at 250 and 500 μ m intervals, the electrical resistance at each interval was measured. On the other hand, the electrical resistance for the continuous tensile tests was recorded continuously throughout the entire test. The measured length, width, and thickness of as-printed lines of 6 mm, 2 mm, and 15 μ m, respectively, were used for the calculation of resistivity. The electrical resistivity increased as the displacement increased regardless of testing modes (i.e., intermittent at different intervals vs. continuous). The electrical resistivity-displacement curves appear to follow exponential growth, indicating that the electrical resistivity increase can be accelerated if the substrate or printed materials is strained more. Although the electrical resistivity increases exponentially, the measured maximum electrical resistivity before the substrate failure was less than ~80 Ω · μ m.

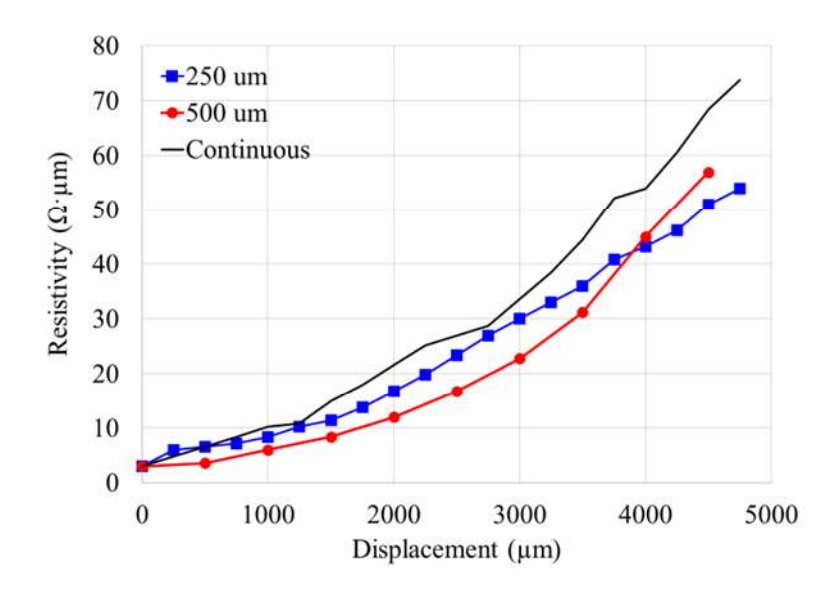


Figure 10 Electrical resistivity-displacement plot of intermittent tensile tests using two different intervals (i.e., $250 \mu m$ and $500 \mu m$) and a continuous tensile test.

The electrical resistivity of the samples fabricated using the process parameters Set #2 (i.e., found to be non-optimal in Section 3.2) were also measured in-situ during tensile tests conducted outside of the SEM. Similar to the process parameters Set #1, the resistivity before applying

tension was less than 5 Ω · μ m. However, the electrical resistivity increased suddenly to over ~100 Ω · μ m at a small displacement of about 300 μ m (or an estimated strain of 3%). This sudden increase in resistivity agrees well with the onset of delamination observed during the in-situ tensile test on the samples fabricated with the process parameters Set #2 (see Figure 9). The exact relationship between the starting point of delamination and resistivity overshooting could not be captured using the proposed testing protocol since the test was not conducted within the SEM to measure resistivity using a multimeter. Future studies will implement in-situ electrical resistance measurement within the SEM by attaching additional probes to the gage of the samples and augmenting the microscope with an additional signal feedthrough. Even though the tensile test conducted outside of SEM could not provide images and resistivity together, it confirmed that while the mechanical properties of the sample were solely contributed by the polyimide substrate, the resistivity was heavily influenced by delamination.

4. Conclusion

A testing protocol to validate adhesion stability under tensile loading was proposed. In-situ tensile tests within the SEM were conducted on polyimide substrates with Ag lines printed by a laser-based additive nanomanufacturing process. With the SEM images and force-displacement data captured during the in-situ tests as well as the force-displacement and electrical resistance-displacement data, the proposed testing protocol to evaluate the print quality of additive nanomanufactured flexible electronics was put forth. The following conclusions were drawn:

Microscopy alone, without in-situ tensile loading, was insufficient to examine the print
quality of additively nanomanufactured metallic lines that would be used in load- or
deformation-bearing applications.

- 2. With the proposed protocol, it was shown that although the two Ag lines printed with different process parameters could have identical surface morphology and elemental mapping, they exhibited significantly different tendencies to delaminate from the substrate.
- 3. The onset of delamination was associated with a sudden increase in the electrical resistivity. The delamination only affected the resistance, not mechanical strength of the sample.

Although this work put forth an effective protocol to test the structural integrity of printed metal layers on polyimide substrates, the exact failure mechanisms call for careful characterization in a future work. In addition, the efficacy of the proposed protocol on substrate materials with significantly different mechanical characteristics, such as silicone rubber, remains to be evaluated.

Acknowledgments

This material is based upon work partially supported by the U.S. National Science Foundation (NSF) under grants No. 1923363 and No. 2134024. SEM imaging was conducted at the National Center for Additive Manufacturing Excellence (NCAME) at Auburn University.

Conflict of interest

The authors declare no conflict of interest.

CRediT author statement

Seungjong Lee: Conceptualization, Methodology, Validation, Formal analysis, Investigation, Data Curation, Writing – Original Draft, Visualization

Zabihollah Ahmadi: Conceptualization, Methodology, Validation, Investigation, Writing – Review & Editing, Visualization

Mikyle Paul: Methodology, Validation, Formal analysis, Investigation, Data Curation, Writing – Review & Editing

Masoud Mahjouri-Samani: Conceptualization, Methodology, Validation, Investigation, Resources, Writing – Review & Editing, Supervision, Funding acquisition

Shuai Shao: Conceptualization, Methodology, Validation, Investigation, Resources, Writing – Review & Editing, Supervision, Funding acquisition

Nima Shamsaei: Conceptualization, Methodology, Validation, Investigation, Resources, Writing

- Review & Editing, Supervision, Project administration, Funding acquisition

References

- [1] K. V Wong, A. Hernandez, A review of additive manufacturing, ISRN Mech, Eng. 1 (2012) 1–10.
- [2] M. Vaezi, H. Seitz, S. Yang, A review on 3D micro-additive manufacturing technologies, International Journal of Advanced Manufacturing Technology. 67 (2013) 1721–1754. https://doi.org/10.1007/s00170-012-4605-2.
- [3] D.S. Engstrom, B. Porter, M. Pacios, H. Bhaskaran, Additive nanomanufacturing A review, J Mater Res. 29 (2014) 1792–1816. https://doi.org/10.1557/jmr.2014.159.
- [4] T. Seifert, E. Sowade, F. Roscher, M. Wiemer, T. Gessner, R.R. Baumann, Additive manufacturing technologies compared: Morphology of deposits of silver ink using inkjet

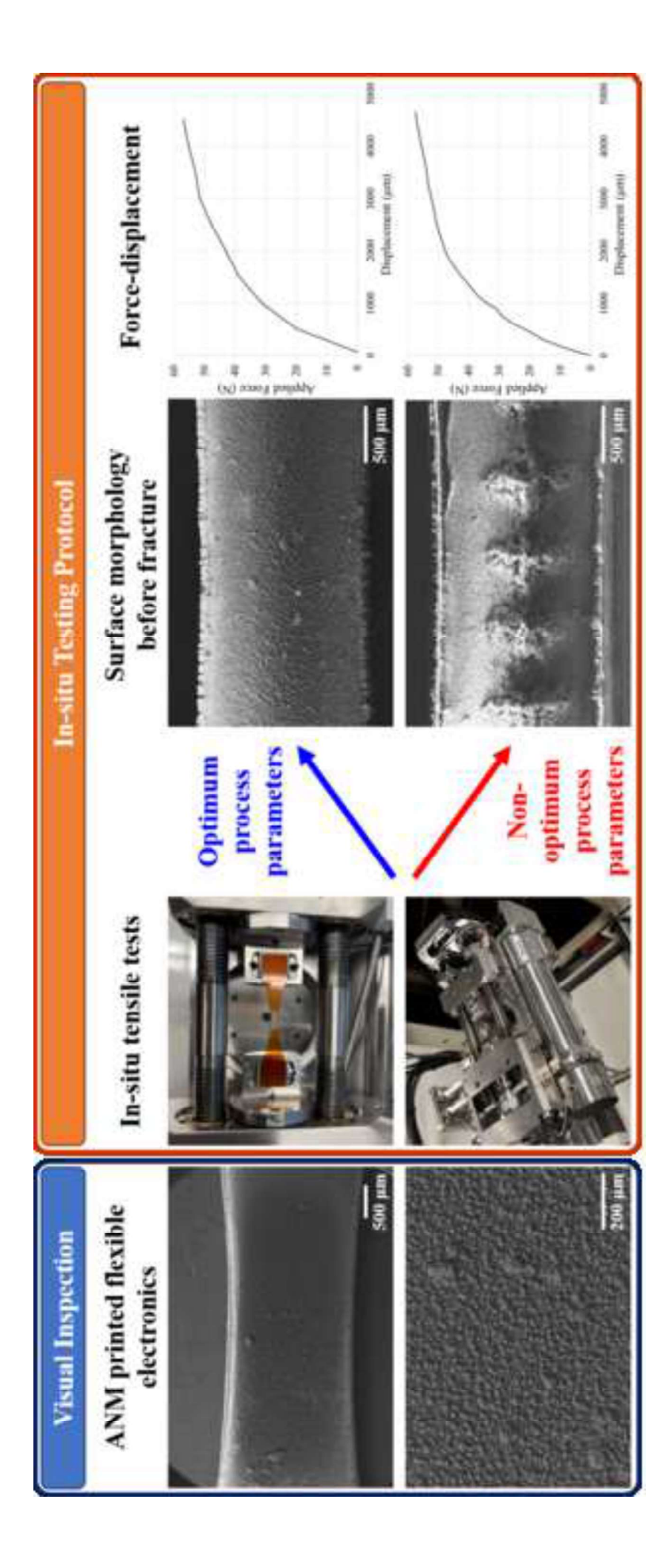
- and aerosol jet printing, Ind Eng Chem Res. 54 (2015) 769–779. https://doi.org/10.1021/ie503636c.
- [5] K.K.B. Hon, L. Li, I.M. Hutchings, Direct writing technology-Advances and developments, CIRP Ann Manuf Technol. 57 (2008) 601–620. https://doi.org/10.1016/j.cirp.2008.09.006.
- [6] B. Lu, H. Lan, H. Liu, Additive manufacturing frontier: 3D printing electronics, Opto-Electronic Advances. 1 (2018) 170004.
- [7] M.S. Hwang, B.Y. Jeong, J. Moon, S.K. Chun, J. Kim, Inkjet-printing of indium tin oxide (ITO) films for transparent conducting electrodes, Mater Sci Eng B Solid State Mater Adv Technol. 176 (2011) 1128–1131. https://doi.org/10.1016/j.mseb.2011.05.053.
- [8] B. Kumar, B.K. Kaushik, Y.S. Negi, Organic thin film transistors: structures, models, materials, fabrication, and applications: a review, Polymer Reviews. 54 (2014) 33–111.
- [9] S.K. Karunakaran, G.M. Arumugam, W. Yang, S. Ge, S.N. Khan, X. Lin, G. Yang, Recent progress in inkjet-printed solar cells, J Mater Chem A Mater. 7 (2019) 13873–13902.
- [10] W. Su, B.S. Cook, Y. Fang, M.M. Tentzeris, Fully inkjet-printed microfluidics: a solution to low-cost rapid three-dimensional microfluidics fabrication with numerous electrical and sensing applications, Sci Rep. 6 (2016) 35111.
- [11] H. Lim, H.S. Kim, R. Qazi, Y. Kwon, J. Jeong, W. Yeo, Advanced soft materials, sensor integrations, and applications of wearable flexible hybrid electronics in healthcare, energy, and environment, Advanced Materials. 32 (2020) 1901924.

- [12] N.J. Wilkinson, M.A.A. Smith, R.W. Kay, R.A. Harris, A review of aerosol jet printing—a non-traditional hybrid process for micro-manufacturing, The International Journal of Advanced Manufacturing Technology. 105 (2019) 4599–4619.
- [13] E.B. Secor, Principles of aerosol jet printing, Flexible and Printed Electronics. 3 (2018) 035002.
- [14] Z. Li, P. Li, G. Chen, Y. Cheng, X. Pi, X. Yu, D. Yang, L. Han, Y. Zhang, Y. Song, Ink engineering of inkjet printing perovskite, ACS Appl Mater Interfaces. 12 (2020) 39082–39091.
- [15] S. Chung, K. Cho, T. Lee, Recent progress in inkjet- printed thin- film transistors, Advanced Science. 6 (2019) 1801445.
- [16] L. Nayak, S. Mohanty, S.K. Nayak, A. Ramadoss, A review on inkjet printing of nanoparticle inks for flexible electronics, J Mater Chem C Mater. 7 (2019) 8771–8795.
- [17] V. Beedasy, P.J. Smith, Printed electronics as prepared by inkjet printing, Materials. 13 (2020) 704.
- [18] C. Zhang, L. McKeon, M.P. Kremer, S.-H. Park, O. Ronan, A. Seral- Ascaso, S. Barwich, C.Ó. Coileáin, N. McEvoy, H.C. Nerl, Additive-free MXene inks and direct printing of micro-supercapacitors, Nat Commun. 10 (2019) 1795.
- [19] Z. Ahmadi, S. Lee, A. Patel, R.R. Unocic, N. Shamsaei, M. Mahjouri- Samani, Dry Printing and Additive Nanomanufacturing of Flexible Hybrid Electronics and Sensors, Adv Mater Interfaces. 9 (2022) 2102569.

- [20] Z. Ahmadi, S. Lee, R.R. Unocic, N. Shamsaei, M. Mahjouri-Samani, Additive Nanomanufacturing of Multifunctional Materials and Patterned Structures: A Novel Laser-Based Dry Printing Process, Adv Mater Technol. 6 (2021). https://doi.org/10.1002/admt.202001260.
- [21] Z. Ahmadi, S. Lee, R.R. Unocic, N. Shamsaei, M. Mahjouri-Samani, Laser-based additive nanomanufacturing of functional hybrid materials, structures, and devices, in: Nanoscale and Quantum Materials: From Synthesis and Laser Processing to Applications 2022, SPIE, 2022: p. PC119900A.
- [22] Z. Ahmadi, S. Lee, N. Shamsaei, M. Mahjouri-Samani, Additive nanomanufacturing of functional materials and devices, in: Laser 3D Manufacturing VIII, SPIE, 2021: p. 116770U.
- [23] H. Kao, C.-H. Chuang, L.-C. Chang, C.-L. Cho, H.-C. Chiu, Inkjet-printed silver films on textiles for wearable electronics applications, Surf Coat Technol. 362 (2019) 328–332.
- [24] Z. Liu, Y. Su, K. Varahramyan, Inkjet-printed silver conductors using silver nitrate ink and their electrical contacts with conducting polymers, Thin Solid Films. 478 (2005) 275–279.
- [25] G.L. Goh, S. Agarwala, W.Y. Yeong, High resolution aerosol jet printing of conductive ink for stretchable electronics, (2018).
- [26] J. Brenneman, D.Z. Tansel, G.K. Fedder, R. Panat, Interfacial delamination and delamination mechanism maps for 3D printed flexible electrical interconnects, Extreme Mech Lett. 43 (2021) 101199.

[27] M. Liu, Q. Zhang, Y. Shao, C. Liu, Y. Zhao, Research of a novel 3D printed strain gauge type force sensor, Micromachines (Basel). 10 (2018) 20.

٠I



Supplementary Material - Video

Click here to access/download

Supplementary Material

Supplemental Video_ANM_in-situ_testing.mp4

Supplementary Material

Click here to access/download

Supplementary Material

Supplemental Material_ANM_in-situ_testing.docx

Declaration of Interest Statement

Declarations of interest: none